BMC Medical Genomics

RESEARCH

Open Access

Transcriptomic analysis reveals key molecular signatures across recovery phases of hemorrhagic fever with renal syndrome

Yuanyuan Hu[1†], Chao Wu[2†], Tuohang Li[3†], Yang Wu[4], Kun Yao[1], Mengtian Zhang[1], Pan Li[1] and Xuzhao Bian[5*]

Abstract

Background Hemorrhagic fever with renal syndrome (HFRS), a life-threatening zoonosis caused by hantavirus, poses significant mortality risks and lacks specific treatments. This study aimed to delineate the transcriptomic alterations during the recovery phases of HFRS.

Methods RNA sequencing was employed to analyze the transcriptomic alterations in peripheral blood mononuclear cells from HFRS patients across the oliguric phase (OP), diuretic phase (DP), and convalescent phase (CP). Twelve differentially expressed genes (DEGs) were validated using quantitative real-time PCR in larger sample sets.

Results Our analysis revealed pronounced transcriptomic differences between DP and OP, with 38 DEGs showing consistent expression changes across all three phases. Notably, immune checkpoint genes like *CD83* and *NR4A1* demonstrated a monotonic increase, in contrast to a monotonic decrease observed in antiviral and immunomodulatory genes, including *IFI27* and *RNASE2*. Furthermore, this research elucidates a sustained attenuation of immune responses across three phases, alongside an upregulation of pathways related to tissue repair and regeneration.

Conclusion Our research reveals the transcriptomic shifts during the recovery phases of HFRS, illuminating key genes and pathways that may serve as biomarkers for disease progression and recovery.

Keywords Hemorrhagic fever with renal syndrome, Transcriptomic alterations, Recovery phases

Background

Hantavirus infection represents an emerging zoonosis with a global increase in both prevalence and geographic spread. The clinical manifestation of hantavirus infection varies significantly depending on the geographic distribution of natural hosts. Notably, hantavirus cardiopulmonary syndrome (HCPS) predominates in the New World, whereas hemorrhagic fever with renal syndrome (HFRS) is prevalent in the Old World [1, 2]. HFRS is predominantly endemic in China, accounting for over 70% of all reported HFRS cases worldwide [3]. HFRS is primarily caused by directly or indirectly inhalation of virus-containing aerosols emitted from the excretions of infected

†Yuanyuan Hu, Chao Wu and Tuohang Li contributed equally to this work.

*Correspondence:
Xuzhao Bian
bianxuzhao@126.com
[1]Medical College, Xijing University, Xi'an 710199, Shaanxi, People's Republic of China
[2]Shapingba Hospital affiliated to Chongqing University (Shapingba District People's Hospital of Chongqing), Chongqing 400030, People's Republic of China
[3]Patent Examination Cooperation Sichuan Center of the Patent Office, CNIPA, Chengdu 610213, Sichuan, People's Republic of China
[4]Xi'an International Medical Center Hospital, Xi'an 710100, Shaanxi, People's Republic of China
[5]School of Public Health, Xi'an Jiaotong University, Xi'an 710049, Shaanxi, People's Republic of China

rodents [4]. HFRS is characterized by acute kidney injury and increased vascular permeability, with mortality rate ranging from 5 to 15% [1]. Currently, there are no approved vaccines or specific treatments for HFRS, and clinical management primarily relies on non-specific supportive therapy.

The clinical progression of HFRS is characterized by a sequential five-stage course: the febrile phase, the hypotensive (low blood pressure) shock phase, the oliguric phase (reduced urine output), the diuretic phase (increased urine output), and finally, the convalescence phase. Each stage exhibits specific clinical manifestations and pathological molecular features that are crucial for diagnosis, management, and prognosis [2, 5]. The current understanding posits that HFRS is predominantly characterized by a dual mechanism involving direct viral infection of the host cells and an indirect overactive immune response. The infection by hantavirus either directly or indirectly activates immune cells, such as CD4+T cells and CD8+T cells, thereby initiating signaling pathways that mediate immune responses. This activation is concurrent with the onset of inflammatory responses, which lead to the activation of the complement system, formation of immune complexes, and production of various pro-inflammatory cytokines. These cytokines further contribute to endothelial dysfunction and increased capillary permeability [6]. To date, Several RNA sequencing studies on HFRS have been conducted, focusing on human umbilical vein endothelial cells (HUVECs) [7], red blood cells (RBCs) [8], and B cells [9], respectively.

In this study, we undertook a comprehensive analysis of the transcriptomic alterations in patients with HFRS across successive recovery stages using RNA sequencing. Our study aimed to delineate key pathways and spotlight genes with significant expression shifts implicated across HFRS's recovery phases. Our findings not only enhance our understanding of HFRS pathology but also opens new avenues for the development of diagnostic tools and therapeutic strategies.

Materials and methods

Patients and ethical approval

All patients involved in this study were admitted to the Xi'an International Center Hospital and diagnosed with HFRS according to the diagnostic criteria outlined in the prevention and treatment strategy of HFRS promulgated by the Ministry of Health of People's Republic of China. Peripheral blood samples were collected from each patient during the oliguric phase (OP), diuretic phase (DP), and convalescent phase (CP), respectively. Exclusion criteria included: (1) Co-infection with other viral or bacterial diseases; (2) Chronic kidney or liver diseases that could confound the study results; (3) Previous history of HFRS or vaccination against hantavirus. Detailed clinical information is summarized in Supplementary Table S1.

RNA extraction, quantification and qualification

Peripheral blood was collected into an anticoagulant tube, and peripheral blood mononuclear cells (PBMCs) were isolated using a commercial Lymphocyte Separation Medium (Beyotime, China) by centrifugation at 700 g for 30 min. Total RNA from the PBMCs was extracted in accordance with the instructions provided by the TRIzol Reagent manual (Life Technologies, California, USA). The concentration and purity of the RNA were determined using a NanoDrop 2000 spectrophotometer (Thermo Fisher Scientific, Wilmington, DE). Additionally, the integrity of the RNA was evaluated using the RNA Nano 6000 Assay Kit on the Agilent Bioanalyzer 2100 system (Agilent Technologies, CA, USA).

Library preparation and sequencing

For library preparation and sequencing, each RNA sample, with an input quantity of 1 μg, underwent library construction using the Hieff NGS Ultima Dual-mode mRNA Library Prep Kit for Illumina (Yeasen Biotechnology, Shanghai, China), as per the provided protocol. Index codes were assigned to each sample for sequence identification. In summary, mRNA was isolated from total RNA utilizing poly-T oligo-attached magnetic beads, followed by synthesis of first-strand cDNA and then second-strand cDNA. DNA fragments had their overhangs blunted and 3' ends adenylated before ligation with NEBNext Adaptors for hybridization preparation. The library fragments underwent purification using the AMPure XP system (Beckman Coulter, Beverly, USA). A final size selection and adaptor-ligated cDNA amplification were conducted using USER Enzyme (NEB, USA) and PCR, employing Phusion High-Fidelity DNA polymerase and primers. PCR products were subsequently purified, and library quality was verified on the Agilent Bioanalyzer 2100 system. Sequencing was performed on the Illumina NovaSeq platform, producing 150 bp paired-end reads, in alignment with Illumina's specifications.

Data quality control and reads mapping to genome

Raw sequencing data in fastq format were subjected to quality control using custom Perl scripts. This preprocessing stage involved the removal of adaptor sequences, reads with poly-N stretches, and low-quality reads, resulting in high-quality, clean data. Concurrently, metrics such as Q20, Q30, GC content, and the level of sequence duplication in the cleaned data were assessed. Subsequent analyses were conducted exclusively on this high-quality, filtered dataset. These processed reads were aligned to the reference genome, with only those achieving a perfect or near-perfect match (up to one mismatch)

being retained for further analysis and annotation. The alignment was performed using the Hisat2 software, specifically designed for mapping to a reference genome.

Differentially expressed genes analysis

Differentially expressed genes (DEGs) between two clinical phases was conducted utilizing DESeq2. The P-values obtained were corrected for multiple hypothesis testing through the Benjamini-Hochberg method to control the false discovery rate. Genes exhibiting an adjusted P-value < 0.01 and a fold change ≥ 2, as determined by DESeq2, were considered as differentially expressed.

Gene ontology and gene set enrichment analysis

Gene Ontology (GO) enrichment and Gene Set Enrichment Analysis (GSEA) were performed to scrutinize the biological pathways enriched among the DEGs using the clusterProfiler package. Top GO and GSEA results between clinical phases were visualized using ggplot2 and ClusterGVis, respectively.

Deconvolution analysis

The abundance of immune cell populations in the samples were estimated using the CibersortX algorithm (https://cibersortx.stanford.edu/) [10]. The input gene expression data were normalized to minimize technical variability across samples. The leukocyte signature matrix (LM22) was used as the reference gene expression matrix, which includes profiles of 22 distinct immune cell types.

Quantitative real-time PCR

Total RNA was reverse transcribed using PrimeScript RT Master Mix (Takara, Japan). The resulting cDNA was quantified with TB Green Premix (Takara). For each gene, the relative mRNA expression levels were normalized to GAPDH expression and calculated using the $2^{-\Delta\Delta CT}$ method. Statistical significance between the two groups was determined using Student's t-test. The primers employed in this study are detailed in Supplementary Table S2.

Results

Transcriptional analysis reveals key genes associated with hantavirus infection recovery

Our initial examination of the correlation among three clinical phases demonstrated that DP and CP shared a closer transcriptional resemblance (Fig. 1A). The deconvolution analysis revealed an increase in T.cells.CD4. memory resting and Macrophages M2 across the three phases, whereas T cells CD4 memory activated, T cells follicular helper, Monocytes, Mast cells resting, and Neutrophils showed a decrease (Fig. 1B). We discerned 974 DEGs between DP and OP, comprising 376 up-regulated and 598 down-regulated genes (Supplementary Table S3); 260 DEGs between CP and DP, with 74 up-regulated and 186 down-regulated (Supplementary Table S4); and 1483 DEGs between CP and OP, including 646 up-regulated and 837 down-regulated genes (Supplementary Table S5) Significantly, 38 genes exhibited consistent alterations across all three clinical phases, indicating their pivotal roles in the recuperation from hantavirus infection (Fig. 1C). Further analysis revealed noteworthy patterns of these genes: eight genes, including *CD83*, *NR4A1*, *DNAJB1*, *FAM71A*, *FCRL6*, *DUSP8*, *HSPA1B*, *HSPA1A*, showed a monotonically increasing trend across three phases. Conversely, four genes, including *IFI27*, *RNASE2*, *MZB1*, *IGKV1-33* demonstrated a monotonically decreasing trend. Additionally, 12 genes were down-regulated between DP and OP and up-regulated between CP and DP, whereas the remaining 14 genes exhibited the reverse trend (Fig. 1D, Supplementary Table S6).

Transcriptional dynamics during the transition from OP to DP

We subsequently explored the transcriptional alterations occurring from OP to DP. Differential expression analysis revealed distinct sets of genes between OP and DP, as delineated in Fig. 2A. Notably, the genes most significantly up-regulated included *LCN10*, *TUBA3D*, *CDRT4*, *SNURF*, *ARC*, *FAT4*, *NR4A1*, *JUN*, *HSPA1B*, and *SLC46A1*, whereas the most down-regulated genes encompassed *CYP19A1*, *SLPI*, *CRISP3*, *CD177*, *MMP8*, *LTF*, *PGLYRP1*, *CEACAM*8, *TCN1*, and *IFI27*. The clustering results of DEGs between OP and DP were depicted in Fig. 2B. GO analysis indicated that up-regulated genes predominantly participated in tissue morphogenesis and renal system development. Conversely, down-regulated genes were primarily associated with the antimicrobial humoral response and myeloid leukocyte-mediated immunity (Fig. 2C). These findings were corroborated by further GSEA analysis, highlighting the gradual restoration of renal system function and the recuperation of immune responses from OP to DP. (Fig. 2D). The interaction between the top 30 up-regulated and down-regulated genes at the protein level is illustrated in Fig. 2E. The up-regulation of *CD83*, *NR4A1*, *JUN*, and *HSPA1B*, as well as the down-regulation of *IFI27*, *RNASE2*, *IFIT1*, and *LCN2*, were confirmed by qPCR (Fig. 2F). Additionally, when compared to normal samples, we found that *CD83* and *NR4A1* levels were significantly elevated (Fig. 2G), suggesting their role in the transition from OP to DP.

Transcriptional alterations during the transition from DP to CP

The transcriptional alteration from DP to CP was subsequently examined. DEGs between DP and CP are

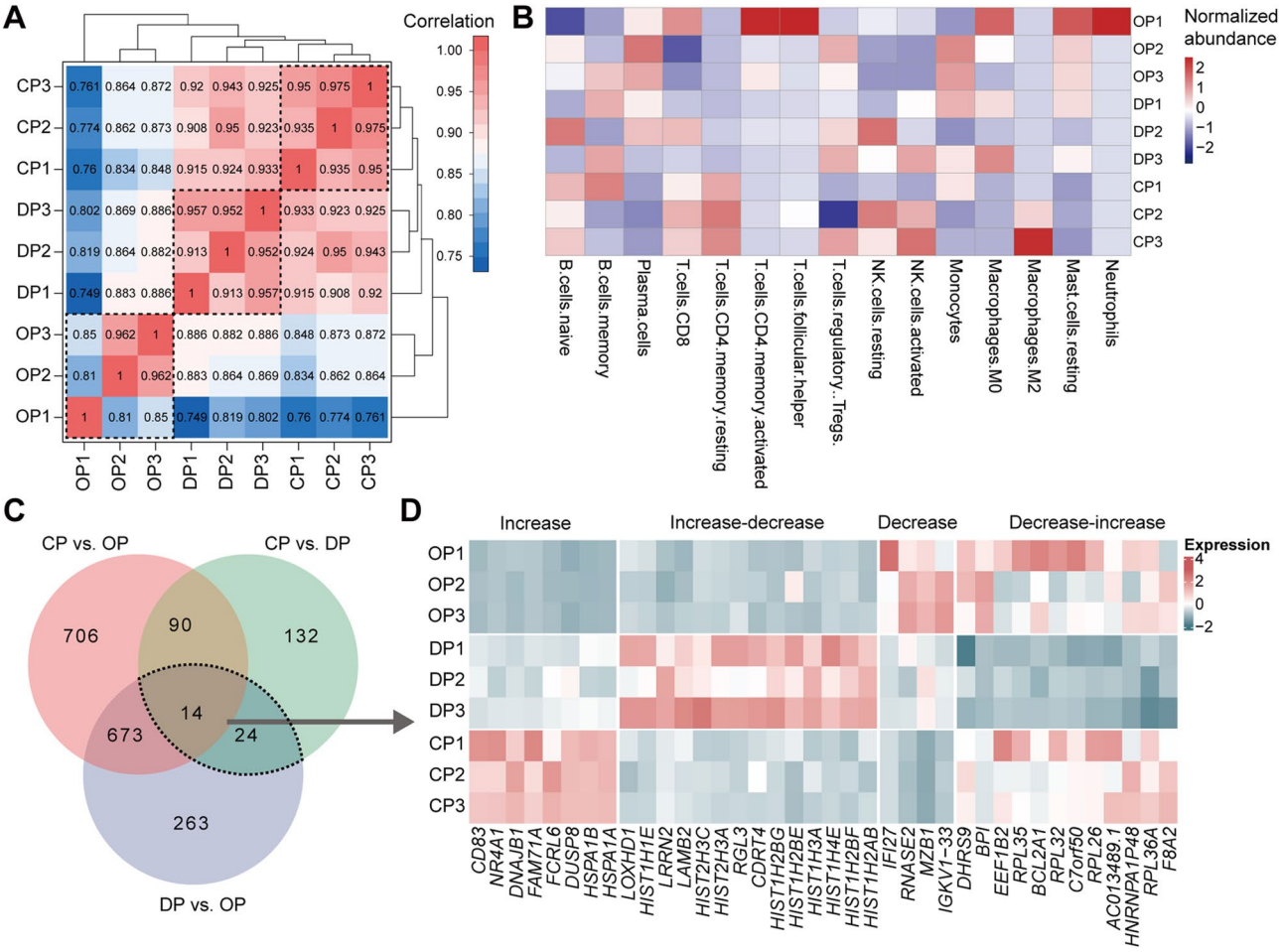

Fig. 1 Transcriptional analysis reveals key genes associated with hantavirus infection recovery. **(A)** Spearman correlation analysis across nine samples spanning three clinical phases. **(B)** The proportion of immune cell types was estimated by CibersortX, the leukocyte signature matrix (LM22) was used as the reference gene expression matrix. **(C)** Venn Diagram illustrating the overlap of DEGs across clinical phases. **(D)** Heatmap shows the genes that are differentially expressed in both DP vs. OP and CP vs. DP comparisons. OP: oliguric phase; DP: diuretic phase; CP: convalescent phase; DEG: differentially expressed gene

presented in Fig. 3A, with *C15orf38-AP3S2*, *AS3MT*, *CD34*, *SHANK1*, *HCAR3*, *NEGR1*, *HCAR2*, *ADGRE3*, *IL1B*, and *CACNA2D3* as the top up-regulated genes, and *RHAG*, *SDC1*, *KCNN3*, *RAB13*, *ADAMTS2*, *IGHV3-72*, *IL1R2*, *MIXL1*, *RNASE1* and *IGF1* as the top down-regulated genes. Clustering of up- and down-regulated DEGs between DP and CP was shown in Fig. 3B. GO analysis showed that genes up-regulated from DP to CP were significantly enriched in functions related to translational initiation and protein targeting to the endoplasmic reticulum, whereas down-regulated genes were chiefly involved in phagocytosis, immunoglobulin production, complement activation, and the adaptive immune response (Fig. 3C). Complementary GSEA further validated these results, emphasizing a transition marked by increased protein synthesis and a moderated immune response from DP to CP (Fig. 3D). The interaction between the top 30 up-regulated and down-regulated genes at the protein level is illustrated in Fig. 3E. The up-regulation of *CD83*, *NR4A1*, *ADGRE3*, and *CCL3*, as well as the down-regulation of *IFI27*, *RNASE2*, *FN1*, and *MZB1*, were confirmed by qPCR (Fig. 3F). Furthermore, we found that *IFI27* levels were significantly elevated in the CP compared to normal samples, whereas *RNASE2* showed no significant change (Fig. 3G).

Discussion

HFRS encompasses a spectrum of clinical manifestations ranging from subclinical to severe symptoms. Early diagnosis is challenging due to the transient and nonspecific nature of initial symptoms [4, 11, 12]. In this study, we conducted a systematic investigation into the transcriptomic dynamics across OP, DP and CP of HFRS. Our findings indicate a greater similarity in the transcriptomic profiles between CP and DP than between DP and OP, highlighting the pronounced alterations occurring

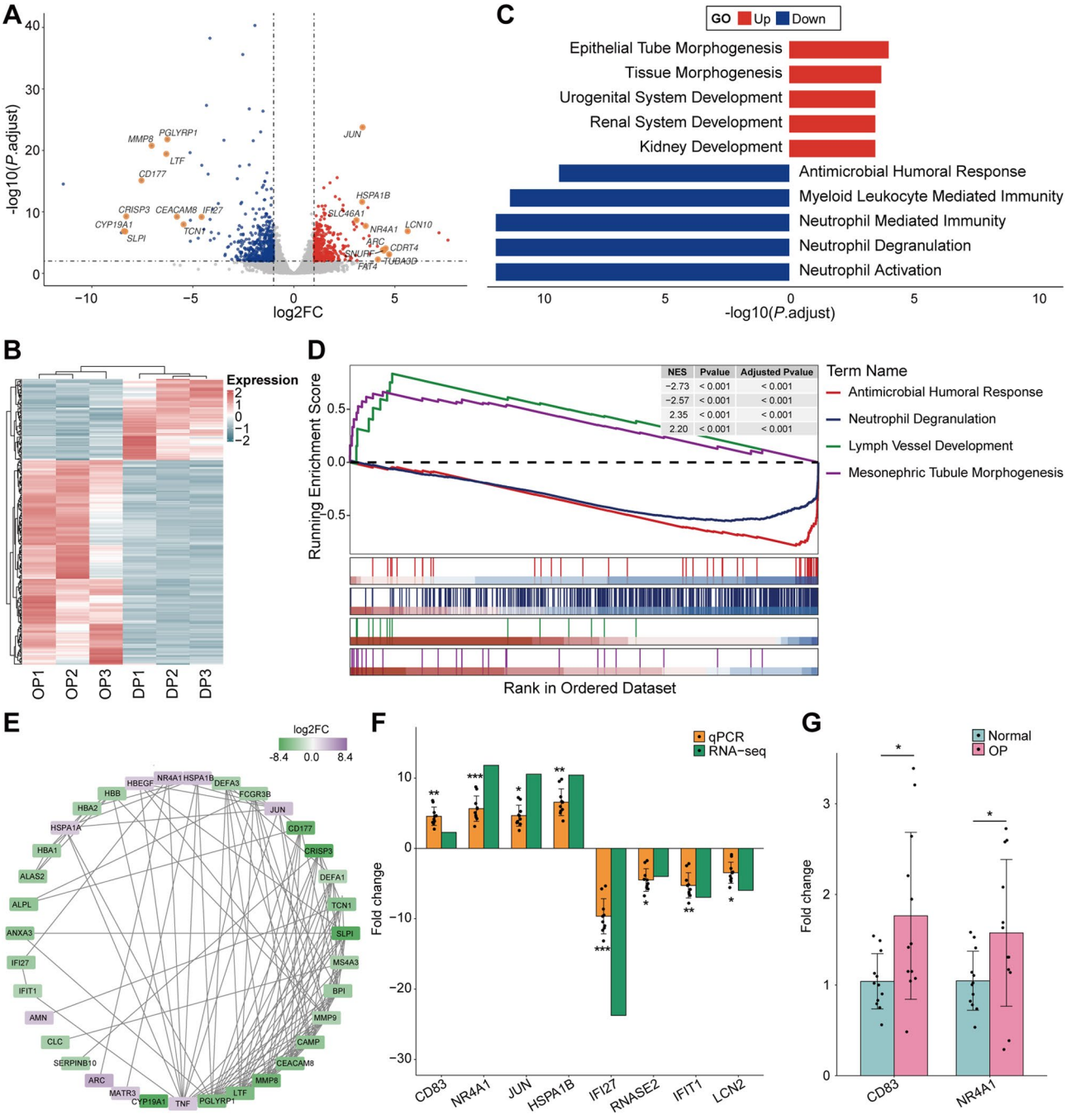

Fig. 2 Transcriptional dynamics during the transition from OP to DP. **(A)** Volcano plot displaying significant DEGs between DP and OP, with top genes labeled. **(B)** Clustering analysis of DEGs between DP and OP. **(C)** Top Gene Ontology (GO) terms enriched among up- and down-regulated genes between DP and OP. **(D)** Gene Set Enrichment Analysis (GSEA) delineates pivotal pathways modulated by DEGs between the DP and OP. **(E)** The interactions of the top 30 up-regulated and down-regulated DEGs were constructed using STRING (https://cn.string-db.org/) and visualized with Cytoscape. The colors represent the log2 fold change of DEGs (DP vs. OP). **(F)** Validation of DEGs during the transition from OP to DP by qPCR, with 12 samples in the OP group and 10 samples in the DP group (DP vs. OP, Student's t-test). **(G)** Expression of *CD83* and *NR4A1* between the OP group ($n = 12$) and normal group ($n = 12$) was measured using qPCR (OP vs. Normal, Student's t-test). OP: oliguric phase; DP: diuretic phase; DEG: differentially expressed gene. Statistical significance is indicated as follows: $^{*}p < 0.05$, $^{**}p < 0.01$, $^{***}p < 0.001$

during the transition from DP to OP. A cohort of 38 genes displayed varied expression patterns throughout the three phases analyzed, underscoring their potential significance. Notably, among the eight genes with a monotonically increasing expression pattern validated by qPCR, *CD83* and *NR4A1* are involved in immune checkpoint regulation, which attenuates the immune response post-infection and during inflammation [13–15].

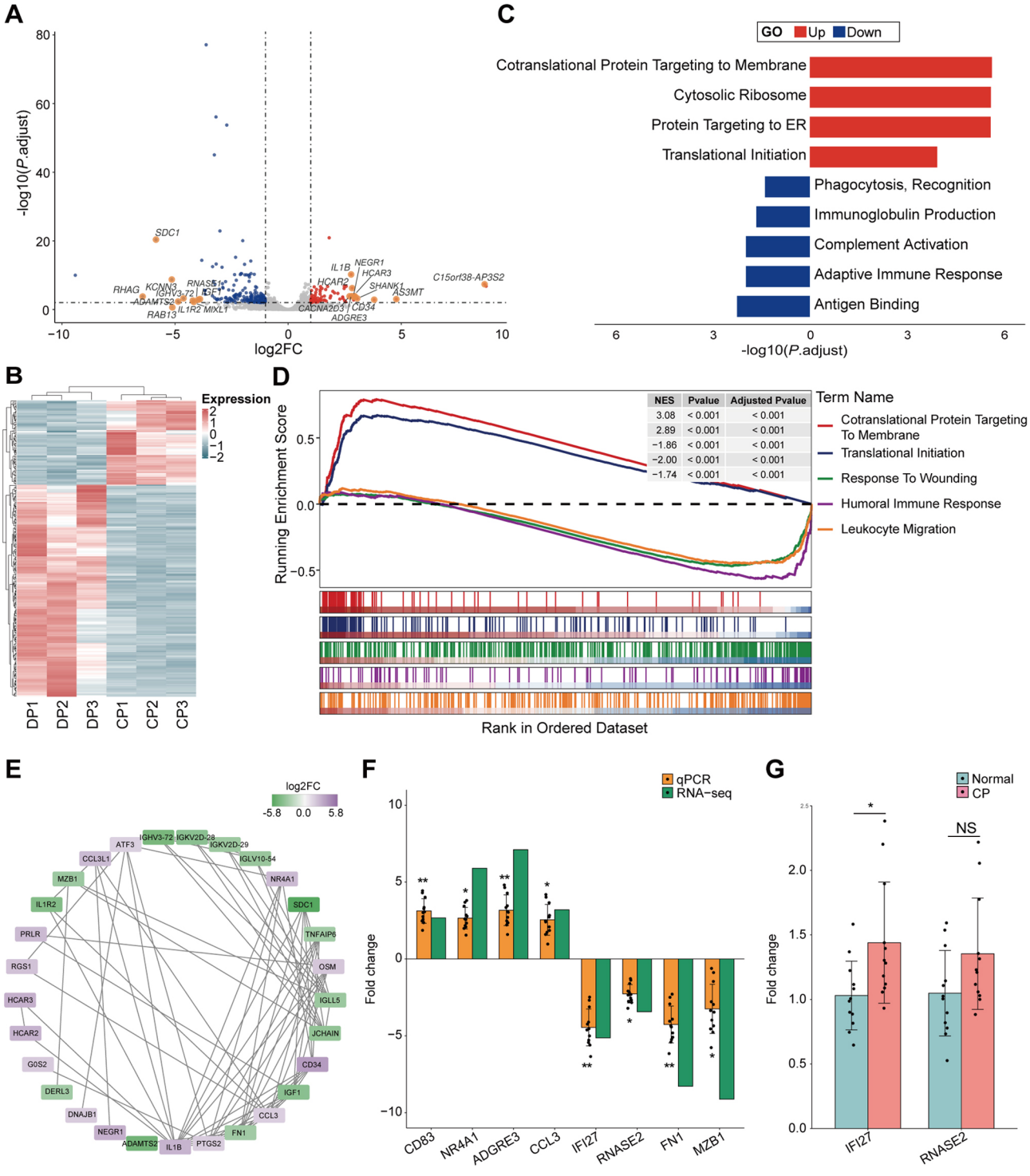

Fig. 3 Transcriptional alterations during the transition from DP to CP. **(A)** Volcano plot illustrating significant DEGs between CP and DP, with top genes highlighted. **(B)** Clustering analysis of DEGs between CP and DP. **(C)** Top Gene Ontology (GO) terms enriched among up- and down-regulated genes between CP and DP. **(D)** Gene Set Enrichment Analysis (GSEA) delineates pivotal pathways modulated by DEGs between the CP and DP. **(E)** The interactions of the top 30 up-regulated and down-regulated DEGs were constructed using STRING (https://cn.string-db.org/) and visualized with Cytoscape. The colors represent the log2 fold change of DEGs (CP vs. DP). **(F)** Validation of DEGs during the transition from DP to CP using qPCR, with 10 samples in the DP group and 12 samples in the CP group (CP vs. DP, Student's t-test). **(G)** Expression of *IFI27* and *RNASE2* between the CP group ($n = 12$) and normal group ($n = 12$) was measured using qPCR (CP vs. Normal, Student's t-test). DP: diuretic phase; CP: convalescent phase; DEG: differentially expressed gene. Statistical significance is indicated as follows: *$p < 0.05$, **$p < 0.01$, ***$p < 0.001$, NS represent not significant

Conversely, of the four genes with a monotonically decreasing expression pattern, *IFI27* and *RNASE2*, also validated by qPCR, are implicated in antiviral and immunomodulatory functions through interactions with innate immune responses [16–19]. Additionally, compared to the normal group, we found that *CD83* and *NR4A1* levels in the OP phase, as well as *IFI27* expression in the CP phase, were significantly higher, indicating their potential as biomarkers for HFRS recovery. These findings suggest a stage-wise alleviation of the immune response, facilitated by the action of immune checkpoint genes.

OP is identified as a critical juncture, with approximately half of the total fatalities occurring during this stage, characterized by elevated levels of creatinine and urea [20]. Our study revealed an upregulation of genes associated with tissue morphogenesis, as well as urogenital and renal system development, indicating a recovery of the renal system during the transition from OP to DP. Expression of *JUN* and *HSPA1B* increased during the transition from the OP to DP, indicating their role in tissue repair and immune response regulation [21–24]. Conversely, the antiviral protein *IFIT1* and the kidney injury marker *LCN2* both showed decreased expression [25, 26]. The rapid humoral innate immune response is crucial for combating virus infections, including hantavirus [9, 27]. Our results revealed that myeloid leukocyte mediated immune response was attenuated during the transition from OP to DP. Meanwhile, deconvolution analysis revealed a decrease in T cells CD4 memory activated, T cells follicular helper, Mast cells resting, and Neutrophils, indicating a reduction in immune response during the recovery phases post-virus infection.

During the transition from DP to CP, an increase in Macrophages M2 suggested an anti-inflammatory response, while the rise in T cells CD4 memory resting indicated that the body had established a long-term immune memory of the virus. Additionally, translational initiation and protein transport processes were enhanced during the transition from DP to CP, suggesting tissue cell repair and regeneration. Concurrently, there was a downregulation of phagocytosis, immunoglobulin production, and complement activation, indicating a return of the immune response to baseline levels during this phase. This result was supported by the down-regulation of *MZB1*, which plays a role in immunoglobulin production and inflammation mitigation [28–30].

In conclusion, our investigation delineates the transcriptomic dynamics across the later three phases in patients recovering from hantavirus infection. We identified 38 dysregulated genes during these transitions, which may serve as biomarkers and therapeutic targets for clinical intervention. The immune response to hantavirus infection was attenuated by immune checkpoint genes, while genes related to tissue repair and regeneration were upregulated, facilitating the restoration of renal system function. Despite the limitations posed by the scarcity of available patient samples across all three recovery phases, our findings provide valuable insights into the molecular mechanisms underlying HFRS recovery, which will facilitate future investigations with larger cohorts and experimental validation.

Supplementary Information

The online version contains supplementary material available at https://doi.org/10.1186/s12920-024-02004-4.

Supplementary Material 1.

Supplementary Material 2.

Supplementary Material 3.

Supplementary Material 4.

Supplementary Material 5.

Supplementary Material 6.

Acknowledgements
Not Applicable.

Author contributions
Xuzhao Bian: Conceptualization, Writing- Reviewing and Editing. Yuanyuan Hu: Formal analysis, Writing - Original Draft preparation. Chao Wu: Data curation, Writing- Original draft preparation. Tuohang Li: Data curation, Visualization. Yang Wu: Resources. Kun Yao: Investigation. Mengtian Zhang: quantitative real-time PCR validation. Pan Li: Writing - Review & Editing.

Funding
This study was supported by Natural Science Research Fund (XJ230109) and Biomedical Research Center Open Project (Swyxkf 202404) of Xijing university.

Data availability
The datasets generated and/or analysed during the current study are available in the Gene Expression Omnibus (GEO) database at https://www.ncbi.nlm.nih.gov/geo/query/acc.cgi? acc=GSE271667 (accession number: GSE271667).

Declarations

Ethics approval and consent to participate
All experiments performed in this study adhered to the ethical guidelines of the Declaration of Helsinki and were approved by the Ethics Committee of Xijing University. Informed consent to participate was obtained from all of the participants in the study.

Consent for publication
Not Applicable.

Competing interests
The authors declare no competing interests.

Received: 4 July 2024 / Accepted: 4 September 2024
Published online: 11 September 2024

References

1. Avsic-Zupanc T, Saksida A, Korva M. Hantavirus infections. Clin Microbiol Infect. 2019;21S:e6–16.
2. Krautkramer E, Zeier M, Plyusnin A. Hantavirus infection: an emerging infectious disease causing acute renal failure. Kidney Int. 2013;83(1):23–7.

3. Wang Y, Xu C, Wu W, Ren J, Li Y, Gui L, et al. Time series analysis of temporal trends in hemorrhagic fever with renal syndrome morbidity rate in China from 2005 to 2019. Sci Rep. 2020;10(1):9609.
4. Bi Z, Formenty PB, Roth CE. Hantavirus infection: a review and global update. J Infect Dev Ctries. 2008;2(1):3–23.
5. Lee GY, Kim WK, No JS, Yi Y, Park HC, Jung J et al. Clinical and immunological predictors of hemorrhagic fever with renal syndrome outcome during the early phase. Viruses. 2022; 14(3).
6. Srikiatkhachorn A, Spiropoulou CF. Vascular events in viral hemorrhagic fevers: a comparative study of dengue and hantaviruses. Cell Tissue Res. 2014;355(3):621–33.
7. Lu S, Zhu N, Guo W, Wang X, Li K, Yan J, et al. RNA-Seq revealed a Circular RNA-microRNA-mRNA Regulatory Network in Hantaan Virus infection. Front Cell Infect Microbiol. 2020;10:97.
8. Zhang J, Tang K, Zhang Y, Ma Y, Zhang C, Hu H, et al. The Presence of circulating nucleated red blood cells is Associated with Disease Severity in patients of hemorrhagic fever with renal syndrome. Front Med (Lausanne). 2021;8:665410.
9. Li Y, Quan C, Xing W, Wang P, Gao J, Zhang Z, et al. Rapid humoral immune responses are required for recovery from haemorrhagic fever with renal syndrome patients. Emerg Microbes Infect. 2020;9(1):2303–14.
10. Newman AM, Steen CB, Liu CL, Gentles AJ, Chaudhuri AA, Scherer F, et al. Determining cell type abundance and expression from bulk tissues with digital cytometry. Nat Biotechnol. 2019;37(7):773–82.
11. Guang MY, Liu GZ, Cosgriff TM. Hemorrhage in hemorrhagic fever with renal syndrome in China. Rev Infect Dis. 1989;11(Suppl 4):S884–890.
12. Jonsson CB, Figueiredo LT, Vapalahti O. A global perspective on hantavirus ecology, epidemiology, and disease. Clin Microbiol Rev. 2010;23(2):412–41.
13. Grosche L, Knippertz I, Konig C, Royzman D, Wild AB, Zinser E, et al. The CD83 molecule - an important Immune Checkpoint. Front Immunol. 2020;11:721.
14. Peckert-Maier K, Langguth P, Strack A, Stich L, Muhl-Zurbes P, Kuhnt C, et al. CD83 expressed by macrophages is an important immune checkpoint molecule for the resolution of inflammation. Front Immunol. 2023;14:1085742.
15. Liu X, Wang Y, Lu H, Li J, Yan X, Xiao M, et al. Genome-wide analysis identifies NR4A1 as a key mediator of T cell dysfunction. Nature. 2019;567(7749):525–9.
16. Ullah H, Sajid M, Yan K, Feng J, He M, Shereen MA, et al. Antiviral activity of Interferon Alpha-Inducible protein 27 against Hepatitis B Virus Gene expression and replication. Front Microbiol. 2021;12:656353.
17. Villamayor L, Lopez-Garcia D, Rivero V, Martinez-Sobrido L, Nogales A, DeDiego ML. The IFN-stimulated gene IFI27 counteracts innate immune responses after viral infections by interfering with RIG-I signaling. Front Microbiol. 2023;14:1176177.
18. Li J, Boix E. Host Defence RNases as antiviral agents against enveloped single stranded RNA viruses. Virulence. 2021;12(1):444–69.
19. Lu L, Li J, Wei R, Guidi I, Cozzuto L, Ponomarenko J, et al. Selective cleavage of ncRNA and antiviral activity by RNase2/EDN in THP1-induced macrophages. Cell Mol Life Sci. 2022;79(4):209.
20. Jiang H, Zheng X, Wang L, Du H, Wang P, Bai X. Hantavirus infection: a global zoonotic challenge. Virol Sin. 2017;32(1):32–43.
21. Florin L, Hummerich L, Dittrich BT, Kokocinski F, Wrobel G, Gack S, et al. Identification of novel AP-1 target genes in fibroblasts regulated during cutaneous wound healing. Oncogene. 2004;23(42):7005–17.
22. Jaiswal J, Egert J, Engesser R, Peyroton AA, Nogay L, Weichselberger V, et al. Mutual repression between JNK/AP-1 and JAK/STAT stratifies senescent and proliferative cell behaviors during tissue regeneration. PLoS Biol. 2023;21(5):e3001665.
23. Atsaves V, Leventaki V, Rassidakis GZ, Claret FX. AP-1 transcription factors as regulators of Immune responses in Cancer. Cancers (Basel). 2019; 11(7).
24. Dubrez L, Causse S, Borges Bonan N, Dumetier B, Garrido C. Heat-shock proteins: chaperoning DNA repair. Oncogene. 2020;39(3):516–29.
25. Pichlmair A, Lassnig C, Eberle CA, Gorna MW, Baumann CL, Burkard TR, et al. IFIT1 is an antiviral protein that recognizes 5'-triphosphate RNA. Nat Immunol. 2011;12(7):624–30.
26. Marques E, Alves Teixeira M, Nguyen C, Terzi F, Gallazzini M. Lipocalin-2 induces mitochondrial dysfunction in renal tubular cells via mTOR pathway activation. Cell Rep. 2023;42(9):113032.
27. Maloney BE, Perera KD, Saunders DRD, Shadipeni N, Fleming SD. Interactions of viruses and the humoral innate immune response. Clin Immunol. 2020;212:108351.
28. Flach H, Rosenbaum M, Duchniewicz M, Kim S, Zhang SL, Cahalan MD, et al. Mzb1 protein regulates calcium homeostasis, antibody secretion, and integrin activation in innate-like B cells. Immunity. 2010;33(5):723–35.
29. Rosenbaum M, Andreani V, Kapoor T, Herp S, Flach H, Duchniewicz M, et al. MZB1 is a GRP94 cochaperone that enables proper immunoglobulin heavy chain biosynthesis upon ER stress. Genes Dev. 2014;28(11):1165–78.
30. Xiong E, Li Y, Min Q, Cui C, Liu J, Hong R, et al. MZB1 promotes the secretion of J-chain-containing dimeric IgA and is critical for the suppression of gut inflammation. Proc Natl Acad Sci U S A. 2019;116(27):13480–9.

Publisher's note